A theoretical investigation into the effect of growth stress variation in tree stems on population measurments

Nicholas Davies[1]

[1]University of Canterbury

August 1, 2018

Introduction

A substantial problem which is not well studied or understood with regard to growth stress is the characterization of the stress field existing within the stem. There is currently no known technology which has the ability to directly or indirectly measure either the surface or volume stress field with a degree of accuracy which would provide insight into the scale of local inhomogeneity. It is suspected, once a reliable technology is developed to investigate the field our understanding and way of thinking about growth stress from both a theoretical and applied view will change significantly. Various hypothetical stress fields based on conservation of energy etc. have been suggested, for a review see Chapter 1.

Currently rudimentary testing technologies such as strain gauges are limited to measuring surface strains with an unknown level of accuracy. There are no current testing procedures which are non-destructive, and hence repeated testing on a unique (all wooden samples are unique) samples is imposable. Most techniques use multiple measurements of surface strain around the stem which are then averaged (Archer, 1987a; Kubler, 1987) to provide a single quantification of 'growth strain' however, the accuracy of any one of these given testing procedures can not be tested as measurement error and variation on the stem surface are completely confounded. The same problem exists for the splitting test as was discussed in Chapter 5, the splitting test is the only growth strain testing procedure fast enough to be used for tree breeding, so calculating its reliability is of practical importance.

A more fundamental problem also exists; the idea that growth strain is usefully quantifiable as a mean surface strain, whether obtained through multiple surface tests or through some geometric averaging as is implicit in the splitting tests. This assertion is particularly problematic for wood scientists who are interested in identifying pieces of timber which are unlikely to bend during sawing whether that be developing in-line screening technology for mills or to assist breeders identifying favorable genetics in breeding programs. In a rudimentary way, the first step to investigating this problem is taken here, by investigating the relationship between surface strain variation with individuals and mean surface strain variation between individuals. Unlikely surface strain profiles are identified and removed and estimates on the reliability of the splitting test and strain gauge tests are made.

Method

Simulating an individual sample

In order to investigate the roll differing surface stress profiles play on the reliability of both the rapid splitting test procedure and 'point' based procedures such as using strain gauges or CIRAD an orthotropic elastic mathematical model of a typical very early selection stem sample was developed. This generic sample was assumed to be a truncated cone with a length of 400 mm, a small end diameter of 34.8 mm and a big end diameter of 39.55 mm. The material of the sample was amused to be orthotropic with longitudinal stiffness coming from *Eucalyptus* argophloia (Chapter 5) the remainder being taken from Gonçalves et al. (2013), or derived as a ratio from the *E.* argophloia longitudinal value. Salome and Netgen (Ribes and Caremoli, 2007öberl1997; **?**) was used to create a mesh of 6436 verticies and 22506 cells to approximate the sample using 3 dimensional tetrahedrons, and a slit from the big end, though the pith with a width of 0.9 mm and a length of 300 mm was added to simulate the splitting test, as can be seen in Figure 1. Further the slit was rotated 90 degrees about the pith and a second mesh created to provide multiple splitting test measurements from each modeled sample.

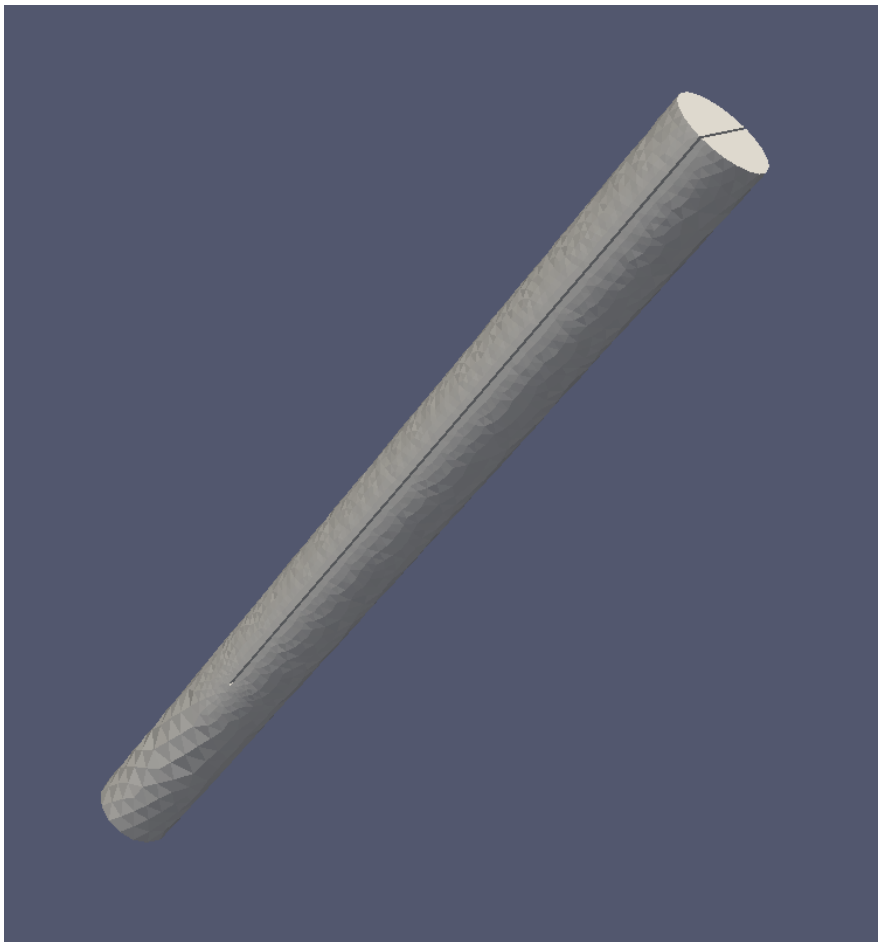

Figure 1: Example of a rapid splitting test sample mesh

Material properties derived from experiments such as in Gonçalves et al. (2013) exist in their native radial coordinate system and hence to be used in a Cartesian coordinate system as was required for some functions of modeling, a transformation between the two was needed. Davies (2014) describes this transformation in Section 3.2.3 using Voigt (engineering) notation to convert the stiffness matrix from radial to Cartesian coordinates at any point in the domain.

Within the stiffness matrix, it was assumed that no taper (i.e. that longitudinal stiffness exists parallel to the vertical axis regardless of the coordinate system), no spiral grain, knots, grain wobble etc. exist and that there is no change in material properties within the volume (i.e. the pith has the same 9 material constants that the periphery has). Further it was assumed that no external forces such as gravity were acting significantly on the simulated samples, the only forcing was the internal stress field.

Traditionally the growth stress field is assumed to be axis-symmetric and follow a curve similar to those presented by (Gillis and Hsu, 1979; Archer, 1987b) etc. Here the stress field existing in a longitudinally ordinated plane from the pith to the periphery can be described by in the same way by Equations 2 to 5. However at every point the value of the surface strain changes, i.e. the stress field is not axis-symmetric is instead governed by Equation 1. Further while the peaks and troughs of the surface strain are 90 degrees apart, their orientation with the splitting test is random and only by chance will peaks/troughs intersect with a cut. This was done as in real world experiments on straight stems it is not known where high or low surface stress is located and hence it can be reasonably assumed that the cut orientation will be randomly aligned with the surface stress pattern. Figure 2 shows some examples of surface strain values around the circumference of some theoretical samples.

Calculating σ_{local} the surface stress for any given point in the stem, where σ_{1-4} is defined in Section and θ is the angular coordinate

$$\sigma_{local} = \begin{cases} \sigma_2 sin(\theta)^2 + \sigma_4 cos(\theta)^2, & \text{if } -\pi \leq \theta < -\frac{\pi}{2} \\ \sigma_2 sin(\theta)^2 + \sigma_3 cos(\theta)^2, & \text{if } -\frac{\pi}{2} \leq \theta < 0 \\ \sigma_1 sin(\theta)^2 + \sigma_4 cos(\theta)^2, & \text{if } 0 \leq \theta < \frac{\pi}{2} \\ \sigma_1 sin(\theta)^2 + \sigma_3 cos(\theta)^2, & \text{if } \frac{\pi}{2} \leq \theta < \pi \end{cases} \tag{1}$$

Defining the radius where compression hits its maximum R_{core}

$$R_{core} = 0.244 R_{max} \tag{2}$$

Where r is the radial coordinate r_v is a virtual radius used only for the Growth stress calculations

$$r_v = \begin{cases} R_{core}, & \text{if } r < R_{core} \\ r, & \text{otherwise} \end{cases} \tag{3}$$

Caluclating G_s the growth stress at any point in the stem

$$G_s = \sigma_{local}(1 + 2.125 log \frac{r_v}{R_{max}}) \tag{4}$$

$$\boldsymbol{\sigma_{gs}} = \begin{bmatrix} 0 \\ 0 \\ G_s \\ 0 \\ 0 \\ 0 \end{bmatrix} \tag{5}$$

Strain can be calculated as follows

$$\boldsymbol{\epsilon} = \frac{1}{2}(\bigtriangledown \boldsymbol{u} + \bigtriangledown \boldsymbol{u}^T) \tag{6}$$

Converted to stress and

$$\boldsymbol{\sigma} = \boldsymbol{C\epsilon} + \boldsymbol{\sigma_{gs}} \tag{7}$$

Strain energy density can then be calculated

$$W = \frac{1}{2}\boldsymbol{\sigma\epsilon} \tag{8}$$

and the total potential energy found

$$\prod = \int_{\boldsymbol{\Omega}} W \, d\boldsymbol{\Omega} \tag{9}$$

By taking the directional derivative of $\prod$ with respect to the change in u and setting it to zero the displacement field u can be calculated at the minimum potential energy.

$$F = \bigtriangledown_{\boldsymbol{u}} \prod(\boldsymbol{u}) = 0 \tag{10}$$

Subject to the Dirichlet boundary condition

$$\boldsymbol{u}|_{\boldsymbol{\Omega_{bc}}} = \begin{bmatrix} 0 \\ 0 \\ 0 \end{bmatrix} \tag{11}$$

$$\boldsymbol{\Omega_{bc}} = \{(x, y, z) \in \boldsymbol{\Omega} : z < 0.001\}$$

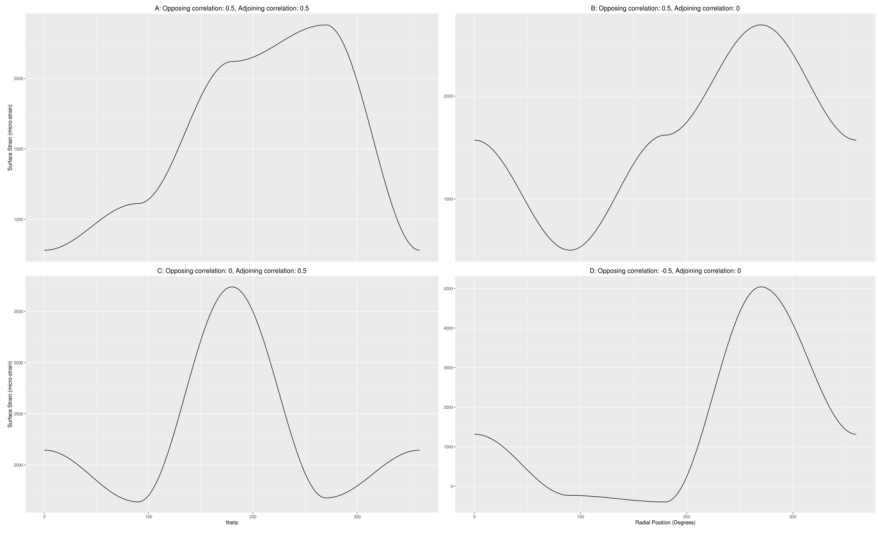

Figure 2: Examples of surface strain profiles

From the resulting deformed coordinate positions, the average displacement of the two halves at the inner edge on the big end of the cut can be calculated (the digital equivalent of the opening measurement in the experimental version of the rapid splitting test). A cut perpendicular (the second mesh) to the first was made, with the same stress field remained identical to that in the first instance. The two openings provide theoretical results of multiple testing of the same individual, without one test influencing another.

Simulating populations

A simulated population here refers to a set of 1000 simulated individual samples which have a (simulated) rapid splitting test mean of 1513 ± 20 $\mu\epsilon$ and a standard deviation of 630 ± 5 $\mu\epsilon$.

In order for the theoretical sample described in Section to be created (which is needed to provide the individuals of the populations), the four input values in Equation 1 need to be defined. For each sample they are calculated from a multivariate normal distribution (Equation 12). The generation of the normal distribution takes the mean matrix which is constant for all samples regardless of their population, and the Covarience matrix which is made up of a population specific input variance and two correlations, C_{Adj} and C_{Opp}, describe how related each of the four evenly spaced stress points on the circumference of the sample are at the populations level (see Figure 2 for a visual representation). The input variance is manipulated to give the output population a standard deviation of 630 ± 5 $\mu\epsilon$ (Note that the output population means are all between 1494 and 1531 $\mu\epsilon$).

$$\begin{bmatrix}\sigma_1\\ \sigma_2\\ \sigma_3\\ \sigma_4\end{bmatrix} = \mathcal{N}\left(\begin{bmatrix}16191994\\ 16191994\\ 16191994\\ 16191994\end{bmatrix}, \begin{bmatrix} \varsigma & C_{Opp}\varsigma & C_{Adj}\varsigma & C_{Opp}\varsigma \\ C_{Opp}\varsigma & \varsigma & C_{Opp}\varsigma & C_{Adj}\varsigma \\ C_{Adj}\varsigma & C_{Opp}\varsigma & \varsigma & C_{Opp}\varsigma \\ C_{Opp}\varsigma & C_{Adj}\varsigma & C_{Opp}\varsigma & \varsigma \end{bmatrix} \right) \tag{12}$$

Where ς is the required input varance for a given population to have an output standard devation of $\pm 630 \mu\sigma$ and:

$$C_{Opp} = \begin{bmatrix} -1 \\ -0.75 \\ -0.5 \\ -0.25 \\ 0 \\ 0.25 \\ 0.5 \\ 0.75 \\ 1 \end{bmatrix} \quad \text{and } C_{Adj} = \begin{bmatrix} -1 \\ -0.75 \\ -0.5 \\ -0.25 \\ 0 \\ 0.25 \\ 0.5 \\ 0.75 \\ 1 \end{bmatrix} \tag{13}$$

By systematically varying C_{Adj} and C_{Opp} (Equation 13) along with input variance populations with the same descriptive statistics (mean and standard deviation) are produced but consist of very different individuals. Note that some populations are not producible statistically, for example C_{Adj} and C_{Opp} can not both be equal

to negative one as no such statistical distribution can exist. For each individual the surface stress profile, true mean stress, and two rapid splitting test values are now known, allowing for comparisons of how well different tests predict each other and the true mean value. Further more, some populations can be removed as unlikely, and from previous experimental work some can be removed not fitting previous experimental evidence. Note plotting and interpolation between the resulting points was conducted in (Team, 2013) using (Auguie, 2017; Akima and Gebhardt, 2016; Wickham, 2016).

Results

The results produced from the models presented in Section where the surface stress is constant (C_{Adj} and C_{Opp} are both one, the typical axis-symmetric assumption when dealing with growth stress in a stem), required an input strain mean and standard deviation of 1442 and 597 $\mu\epsilon$ to produce an output population mean and variance of 1520 and 629 $\mu\epsilon$ respectively. The differences indicate that either the testing procedure or the model slightly overestimate surface strain from split opening. Note that because both the predicted opening and the surface stress at a given point are known to machine precision it is assumed there is no measurement error in either the opening or strain gauge measurements, this is in contrast to experimental methods where such measurement error does exist with an unknown magnitude (Chapter 5 attempts to quantify this error). Figure 3 shows the required input strain standard deviation to give the output population standard deviation of 630 ± 5 $\mu\epsilon$.

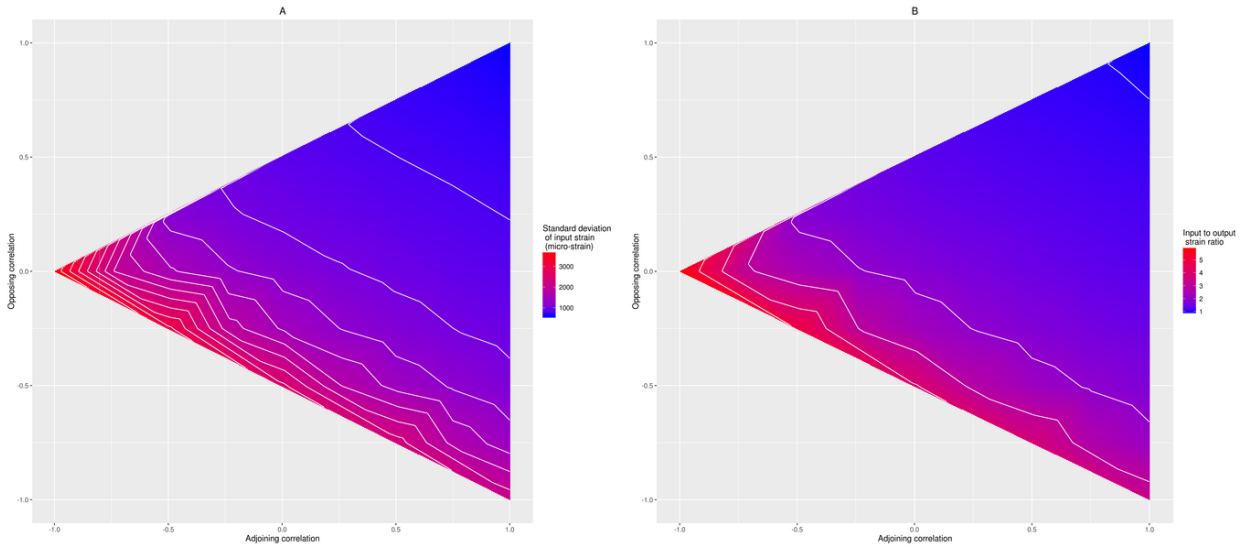

Figure 3: Strain standard deviation input (A)and input to output ratio (B) with respect to surface point strain corrolations

Investigation of splitting test accuracy over different surface stress fields yields Figure 4 when comparing how well one splitting test result predicts the perpendicular result on the same sample. In contrast Figure 5 shows how well the test predicts the true input surface stress mean. The contour lines on Figures (3 to 11) are spaced 0.1 apart where the color gradient represents a correlation (Sub-figure A) and 250 $\mu\epsilon$ where the color gradient represents a standard deviation (Sub-figure B).

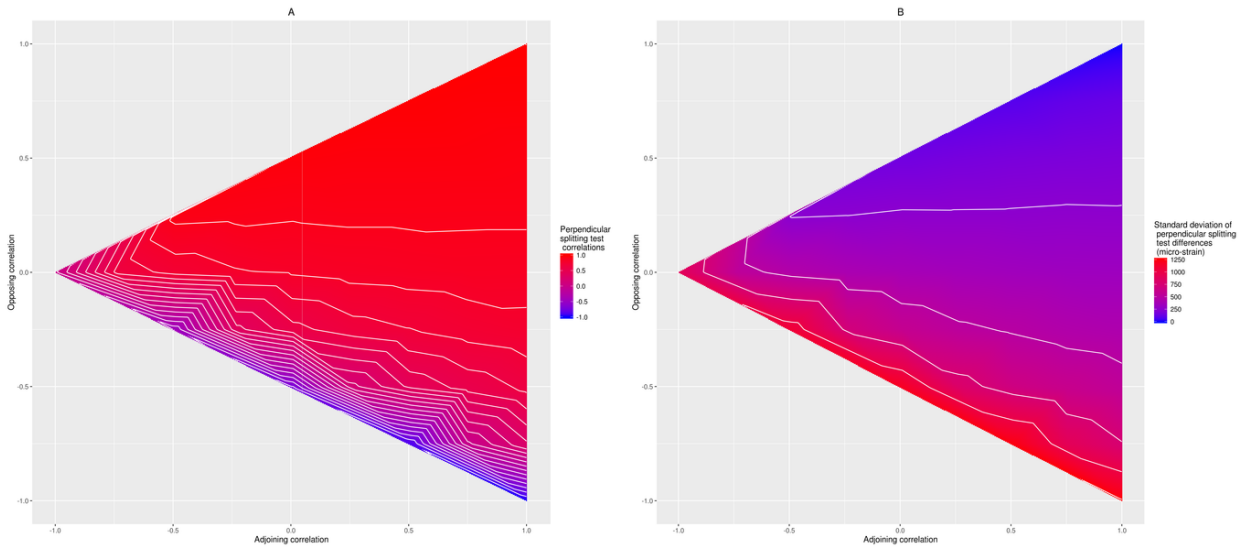

Figure 4: Correlation (A) and standard deviation (B) of the differences between perpendicular splitting tests.

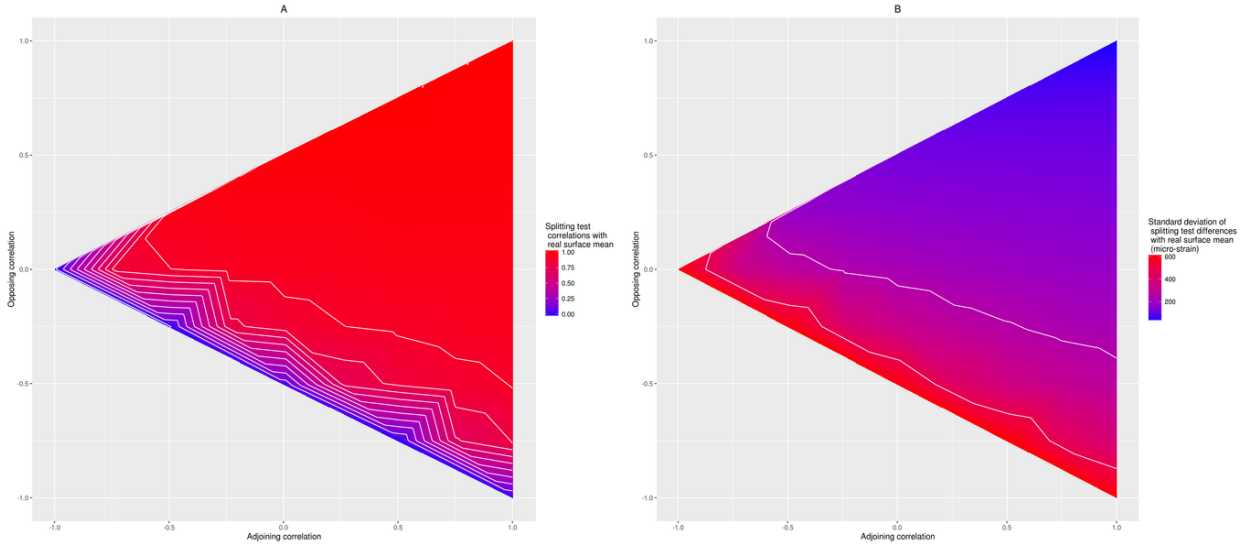

Figure 5: Correlation (A) and standard deviation (B) of the differences between the real surface strain mean and splitting test predictions.

Chauhan and Entwistle (2010b) used two strain gauges placed perpendicular to the splitting test cut (visually in Figure 6, the cut is through the pith, and the red strain gauges are placed perpendicular to it) and presented a correlation of 0.92 between predicted opening by the strain gauges and the measured opening. The same test was conducted here with Figure 7 showing the results, as is expected from the geometry of the testing procedure, the correlations are high. In contrast, Figure 5 shows how well the splitting test predicts the true surface strain, and Figure 8 shows the how well two strain gauges placed 180 degrees apart predict the true mean surface strain. Figures 9 to 11 show how well various numbers of strain gauges predict the true surface stress mean.

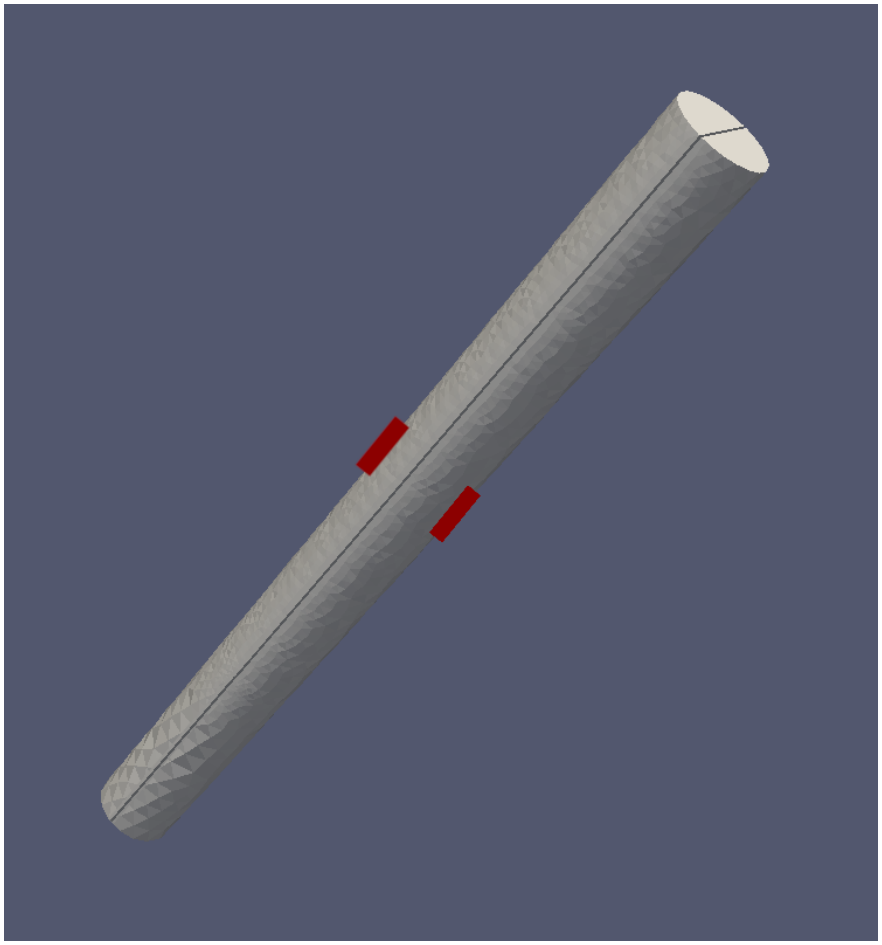

Figure 6: An representation of the experimental setup in Chauhan and Entwistle (2010a)

More typically, 4 or 8 strain gauges (or CIRAD) are placed at equal spacing around a stem, Figures 9 through 11 show the relationship between the number of gauges and how well they predict the real surface stress mean for various surface stress profiles.

Discussion

When C_{Opp} and C_{Adj} are both equal to one, there is no variation of stress in the stem. Interestingly the input axis-symmetric surface strain of 1442 rises to 1520 $\mu\epsilon$ and the population variance rises from 597 (surface) to 629 $\mu\epsilon$ (splitting test) indicating the rapid splitting test slightly over-predicts the real surface strain. These results suggest the rapid splitting test will predict a surface strain approximately 5% higher than the true value (although this may change depending on the magnitude of the strain). Note that this value is insignificant compared to the errors discussed below. Figure 3 A shows the relationship between the surface point relatedness and the required input strain distribution standard deviation, B shows the same

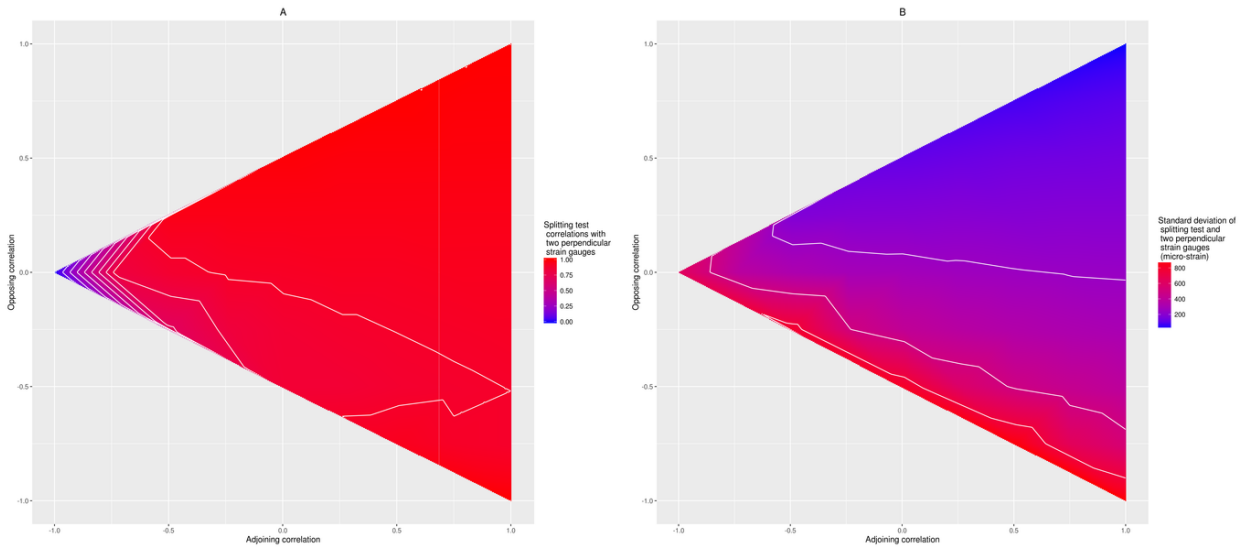

Figure 7: Correlation (A) and standard deviation (B) of the differences between the splitting test and the average of two strain gauges placed as per Chauhan and Entwistle (2010a).

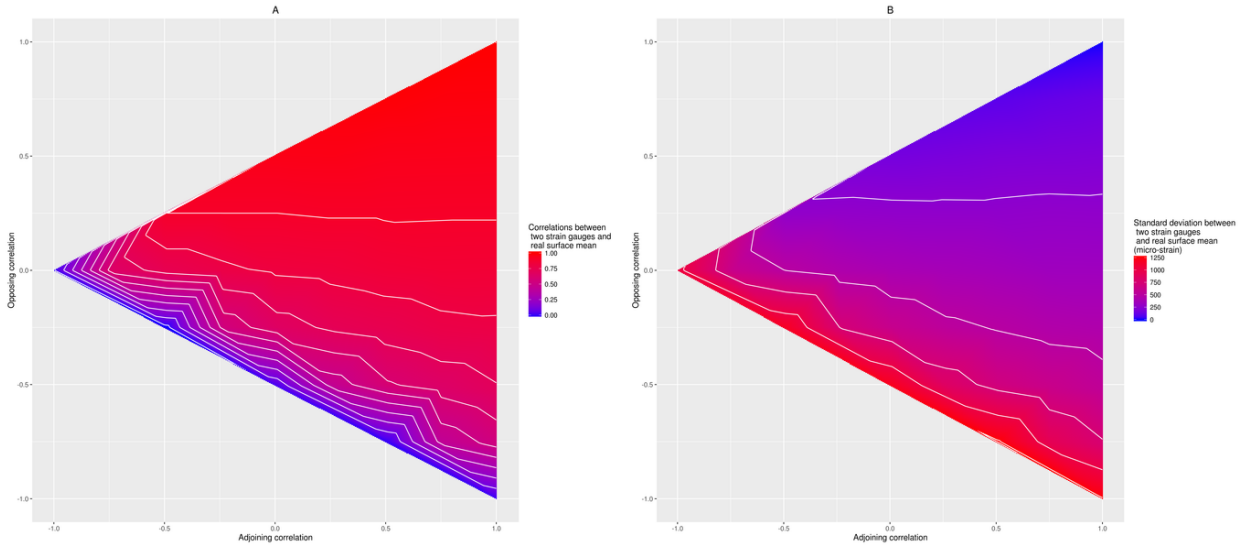

Figure 8: Correlation (A) and standard deviation (B) of the differences between the real surface strain mean and the average of two strain gauges placed 180 degrees apart.

information but presented as a ratio of the output population strain standard deviation (the input strain is divided by 630 $\mu\epsilon$). It can be seen in Figure 3 that as the correlation between surface points reduces and becomes negative, the required input strain standard deviation increases to provide the same output population statistics. This is important as it provides context for how much surface variation must exist for given surface point relationships to obtain a typical output population. The top contour in Figure 3 B is the 1:1 contour, where the input strain is equal to the output population strain, it is slightly offset from the top corner due to the bias discussed above. The 2:1 contour is where the standard deviation of the input strain was required to be twice that of the output population strain. Note that on this contour the within stem variance is three times that of the population variance.

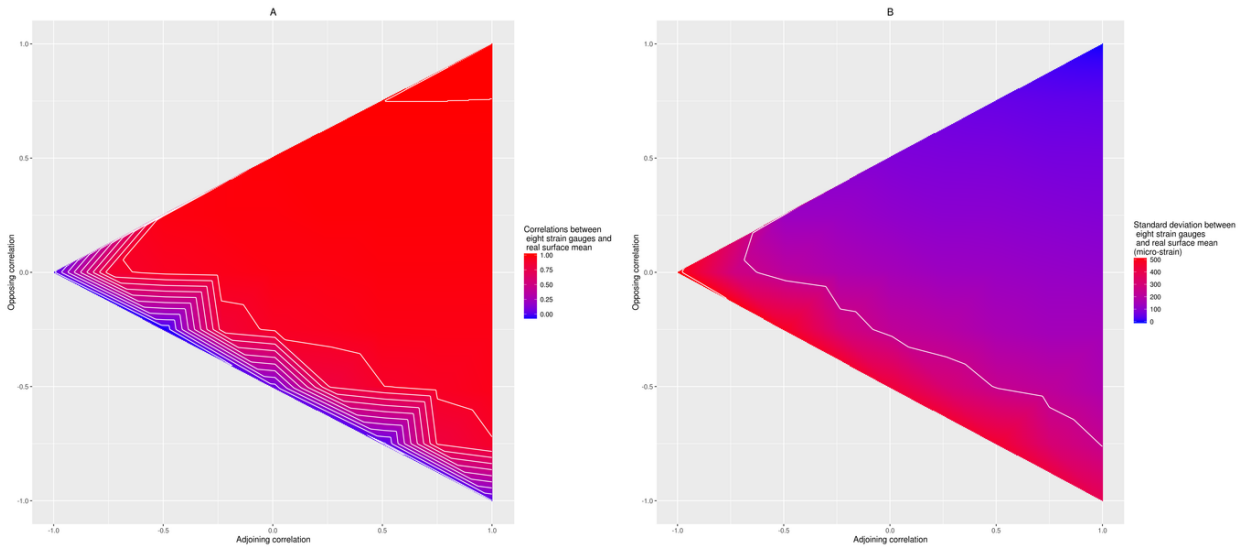

Figure 9: Correlation (A) and standard deviation (B) of the differences between the real surface strain mean and the average of eight strain gauges placed 45 degrees apart.

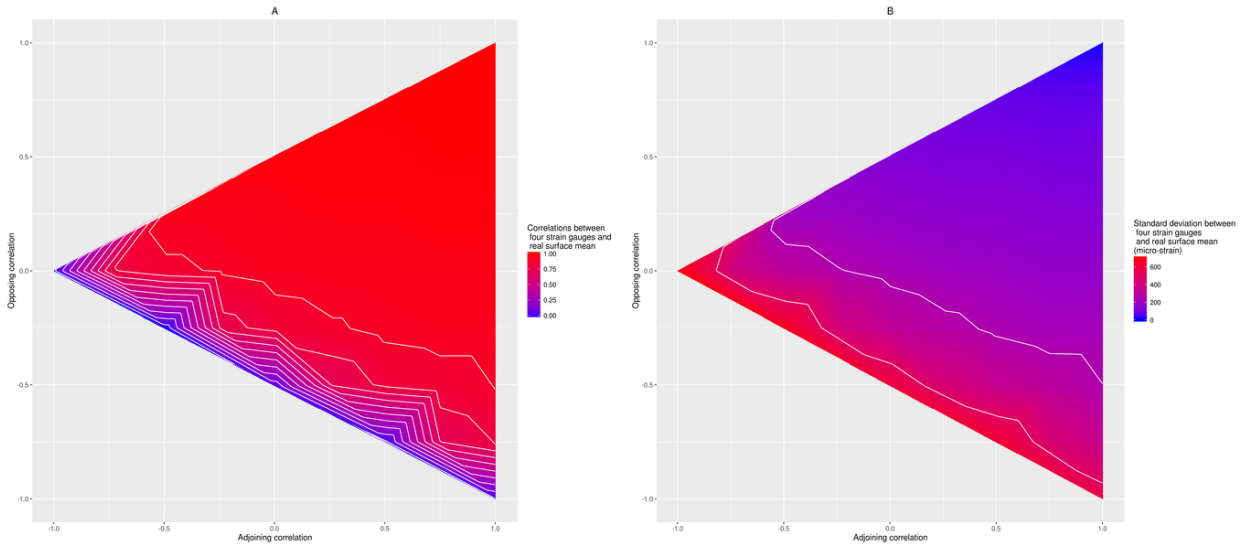

Figure 10: Correlation (A) and standard deviation (B) of the differences between the real surface strain mean and the average of four strain gauges placed 90 degrees apart.

Chapter 5 outlined an experimental procedure for predicting the precision of the the splitting test, and particularly the magnitude of change in surface strain which is associated with the arbitrary angle of the cut during the splitting test. Experimentally the correlation between the two quartering tests (0.89) and the estimated standard deviation of the difference distribution (300 $\mu\epsilon$). When the experimental method is compared to the closest theoretical example (Figure 4), it is seen that the experimental results both must exist when C_{Opp} is grater than 0 and C_{Adj} is greater than -0.5. When Chauhan and Entwistle (2010a) is repeated within the theoretical framework (Figure 7) a similar conclusion can be drawn, however slightly

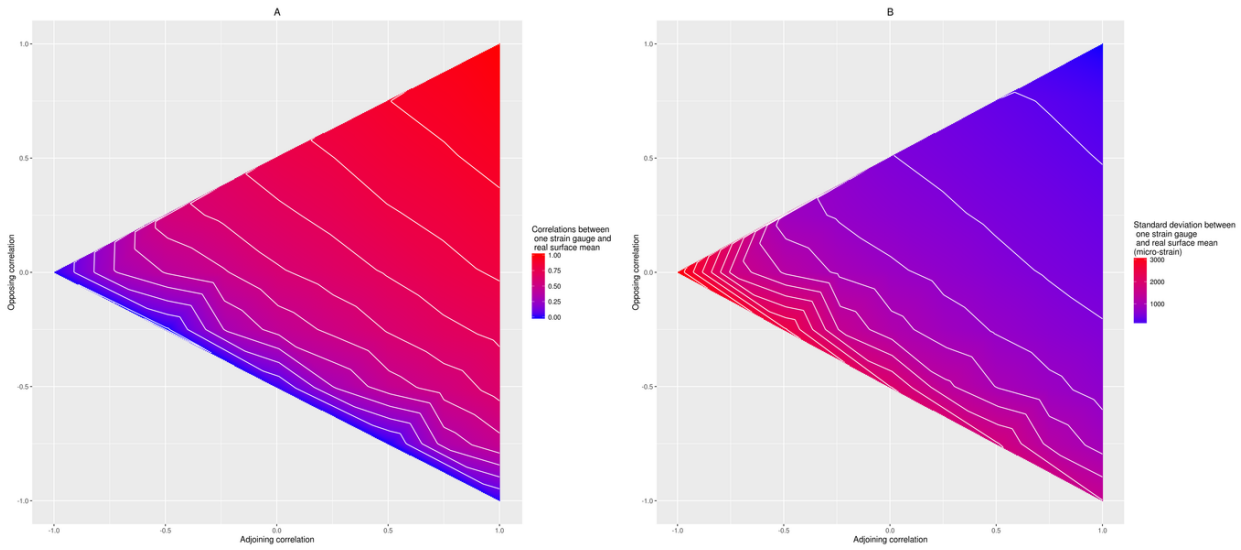

Figure 11: Correlation (A) and standard deviation (B) of the differences between the real surface strain mean and a single randomly paced strain gauge.

negative C_{Opp} and high C_{Adj} populations could also be included. Following this, two population sets will be refereed to, the *full population set* consisting off all of the populations used to make the above figures, and the *limited population set*, the set which exists inside the lower bounds suggested by the experimental work in Chapter 5.

When perpendicular splitting test results are compared it can be seen that most populations produce a moderate or higher correlation between two perpendicular tests, when using the limited population set the correlations are markedly improved, Figure 12 shows the density curves for each population set. While the correlations between perpendicular splitting tests are fairly high, Figure 12 shows even with the high correlations within the limited population set, there can still be significant standard deviations of the differences between the two tests, implying a high error when attempting to identify individuals as superior. If instead the comparison is made between splitting test results and the true surface strain mean, again Figure 13 shows the destiny comparisons between the full and limited population sets. Most striking here is the substantial movement toward the higher end of strain correlations of both population sets. This can also be seen in Figure 5 where the standard deviation of the difference distribution approximately halves for all populations, along with the correlation between splitting test and true surface strain correlations approximately doubling, compared to Figure 4. The implication being that the accuracy of the splitting test my be higher than the precision suggested in Chapter 5.

In Chauhan and Entwistle (2010a) the method used to lend credibility to the splitting test method involved placing two strain gauges perpendicular to splitting test cut as can be seen in Figure 6. Here that experiment was repeated using the computer models over the various populations outlined. Figure 7 shows a high correlation and low difference distribution standard deviation between the two gauges and the splitting test, as is expected given the experimental design. However when two randomly (evenly spaced) orientated strain gauges are used to predict the real mean surface strain (Figure 8) it can be seen there is a large associated error (larger than when the splitting test is used to predict it), indicating that this method is not a good method to test how reliably the splitting test estimates the real mean surface strain.

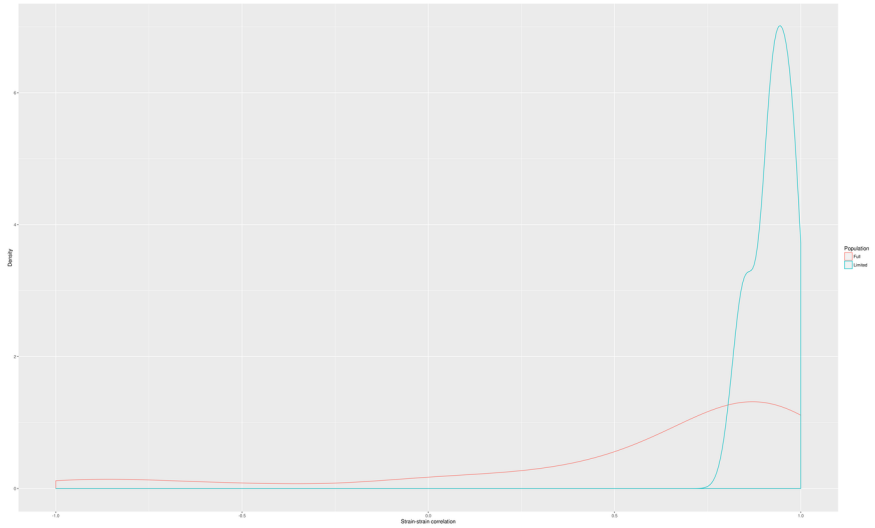

Figure 12: Density distribution of the correlations between perpendicular splitting test measurements for the two population sets

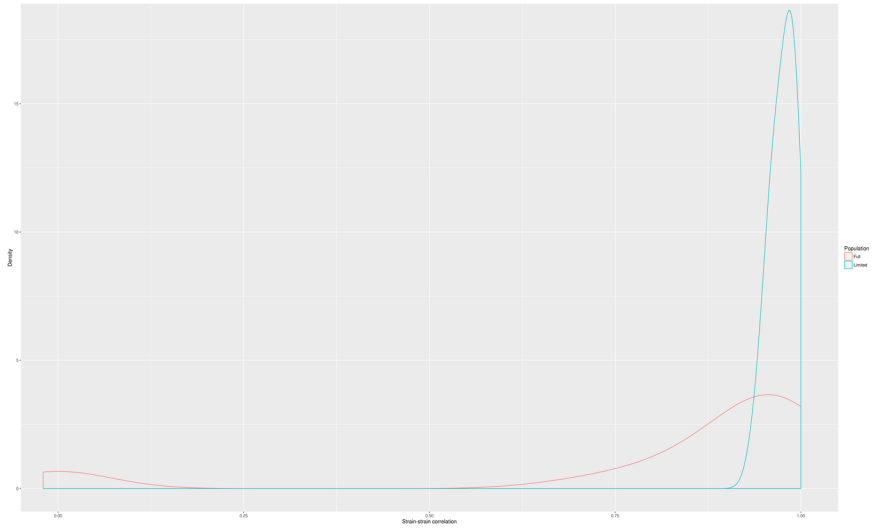

Figure 13: Density distribution of the correlations between the real mean surface strain and splitting test measurements for the two population sets

As one would suspect the more evenly spaced gauges placed on the surface of a sample, the more accurately the average gauge value will predict the true surface strain mean, as can be seen in Figures 8 to 11. Comparing the relationships of the splitting test and 4 gauges with the real surface mean, (Figures 5 and 10 respectively) the results are quite comparable. The splitting test produces a mean standard deviation of 262 $\mu\epsilon$ and the four strain gauges of 260 $\mu\epsilon$ in the full populations set and 132 $\mu\epsilon$ and 128 $\mu\epsilon$ in the limited set, while using eight gauges produces an advantage over both (184, 100 $\mu\epsilon$).

The results for the full and limited populations are presented in Table 1 with maximum, minimum and mean values. Of particular interest is the limited population set perpendicular splitting test standard de-

viation (the standard deviation of the difference between the two splitting tests performed on the same sample) is 244 $\mu\epsilon$, which as a 95% confidence interval is 478 $\mu\epsilon$, while this is lower than the 589 $\mu\epsilon$ found using the experimental method in Chapter 5, it may just be an indication that some of the populations with fairly consistent surface strains are over represented compared to the Chapter 5 data (or that the experimental data was incorrectly specifying some measurement error with rotational error). Biologically it seams unlikely that completely consistent surface strain profiles exist but a lower bound on 95% confidence intervals of approximately ± 480 $\mu\epsilon$ on the repeatability of a rapid splitting test on samples similar to those represented here seams reasonable (ignoring measurement error). The lower bound (it is likely to be less acurate) on the 95% confidence interval of the prediction of the real surface strain mean from the rapid splitting test is $\pm$ 281 $\mu\epsilon$. Given the limited population set requires a mean input surface strain of 877.7 $\mu\epsilon$ to get an output population with a standard deviation of 630 $\mu\epsilon$ the intra and inter stress variances are partitioned approximately in half i.e. the standard devation within a stem (611 $\mu\epsilon$) is approximately equal to the standard devation between stems (630 $\mu\epsilon$), within the limited population set. As above however, the within stem variation is probably a little higher in the experimental work from Chapter 5.

Population	Full			Limited		
	Mean	Minimum	Maximum	Mean	Minimum	Maximum
Mean strain input (micro-strain)	1435.27	1417	1449	1439.48	1423	1449
Standard deviation strain input (micro-strain)	1270.71	597	3680	877.7	597	1527
Perpendicular splitting test (micro-strain)	472.34	0	1263	243.83	0	455
Perpendicular splitting test correlations	0.59	-1	1	0.91	0.74	1
Splitting test difference SD with real value (micro-strain)	261.93	32	634	143	32	279
Splitting test correlation with real value	0.81	-0.02	1	0.97	0.9	1
Entwistle method difference SD (micro-strain)	338.17	32	896	177.3	32	322
Entwistle method correlation	0.9	-0.01	1	0.96	0.88	1
Single strain gauge difference SD (micro-strain)	861.32	0	3181	500.48	0	1208
Single strain gauge correlation	0.58	-0.01	1	0.76	0.41	1
Two strain gauges difference SD (micro-strain)	491.78	0	1265	257.7	0	497
Two strain gauges correlation	0.71	-0.03	1	0.9	0.74	1
Four strain gauges difference SD (micro-strain)	259.66	0	729	141.48	0	302
Four strain gauges correlation	0.8	-0.05	1	0.97	0.88	1
Eight strain gauges difference SD (micro-strain)	184.27	0	520	100.35	0	211
Eight strain gauges correlation	0.84	-0.07	1	0.98	0.93	1

Table 1: Full and limited population set statistics for the verious testing procedured investigated.

Conclusion

A computational model was developed to investigate how variation of surface growth stress around the stem effects results of the splitting test and the mean values of various numbers of strain gauges. By modeling

multiple populations with differing stress relationships around the stem surface and comparing the results to previous work, realistic bounds were able to be estimated for the relatedness of surface stress points. The repeatability of the splitting test under rotation was investigated and a similar, although lower result as Chapter 5 was found (95% confidence interval on the difference distribution of ± 480 $\mu\epsilon$). A lower bound (i.e. it is likely to be less accurate than) on the 95% confidence of a splitting test result predicting the real mean surface strain for similar populations was estimated to be $\pm$ 281 $\mu\epsilon$. Further, it was concluded that the rapid splitting test provides a similar accuracy in predicting mean surface strain on a sample as using four evenly spaced strain gauges (a difference distribution standard deviation of 262 $\mu\epsilon$ for the splitting test in the full populations set and 132 $\mu\epsilon$ for a more realistic limited set).

References

Hiroshi Akima and Albrecht Gebhardt. *akima: Interpolation of Irregularly and Regularly Spaced Data*, 2016. URL https://CRAN.R-project.org/package=akima. R package version 0.6-2.

Robert R. Archer. *Growth Stresses and Strains in Trees*. Springer Berlin Heidelberg, 1987a. doi: 10.1007/978-3-662-02511-6. URL https://doi.org/10.1007%2F978-3-662-02511-6.

Robert R. Archer. *Growth Stresses and Strains in Trees*. Springer Berlin Heidelberg, 1987b. doi: 10.1007/978-3-662-02511-6. URL https://doi.org/10.1007%2F978-3-662-02511-6.

Baptiste Auguie. *gridExtra: Miscellaneous Functions for Grid Graphics*, 2017. URL https://CRAN.R-project.org/package=gridExtra. R package version 2.3.

Shakti Chauhan and Kenneth Entwistle. Measurement of surface growth stress in Eucalyptus nitens Maiden by splitting a log along its axis. *Holzforschung*, 64(2), jan 2010a. doi: 10.1515/hf.2010.022. URL https://doi.org/10.1515%2Fhf.2010.022.

Shakti Chauhan and Kenneth Entwistle. Measurement of surface growth stress in Eucalyptus nitens Maiden by splitting a log along its axis. *Holzforschung*, 64(2), jan 2010b. doi: 10.1515/hf.2010.022. URL https://doi.org/10.1515%2Fhf.2010.022.

Nicholas Tuatahi Davies. Reverse Engineering the Tree. 2014.

P. P. Gillis and C. H. Hsu. An elastic plastic theory of longitudinal growth stresses. *Wood Science and Technology*, 13(2):97–115, 1979. doi: 10.1007/BF00368603. URL http://dx.doi.org/10.1007/BF00368603.

Raquel Gonçalves, Alex Julio Trinca, and Bruno Piva Pellis. Elastic constants of wood determined by ultrasound using three geometries of specimens. *Wood Science and Technology*, 48(2):269–287, nov 2013. doi: 10.1007/s00226-013-0598-8. URL https://doi.org/10.1007%2Fs00226-013-0598-8.

H. Kubler. Growth stresses in trees and related wood properties. *Forestry Abstacts*, 48(3):131–189, 1987.

Andre Ribes and Christian Caremoli. Salome platform component model for numerical simulation. In *31st Annual International Computer Software and Applications Conference - Vol. 2 - (COMPSAC 2007)*. IEEE, jul 2007. doi: 10.1109/compsac.2007.185. URL https://doi.org/10.1109%2Fcompsac.2007.185.

R Core Team. *R: A Language and Environment for Statistical Computing*. R Foundation for Statistical Computing, Vienna, Austria, 2013. URL http://www.R-project.org/.

Hadley Wickham. *ggplot2: Elegant Graphics for Data Analysis*. Springer-Verlag New York, 2016. ISBN 978-3-319-24277-4. URL http://ggplot2.org.